Journal of Alloys and Compounds 520 (2012) 42–51

Contents lists available at SciVerse ScienceDirect

Journal of Alloys and Compounds

journal homepage: www.elsevier.com/locate/jallcom

Magnetic properties of $Li_xNi_yMn_yCo_{1-2y}O_2$ ($0.2 \leq 1-2y \leq 0.5$, $0 \leq x \leq 1$)

A. Mauger[a,*], F. Gendron[b], C.M. Julien[c]

[a] Institut de Minéralogie et Physique de la Matière Condensée, Université Pierre et Marie Curie, Case courrier 115, 4 Place Jussieu, 75252 Paris Cedex 05, France
[b] Institut des Nanosciences de Paris, Université Pierre et Marie Curie, 4 Place Jussieu, 57252 Paris Cedex 05, France
[c] Laboratoire de Physicochimie des Electrolytes, Colloïdes et Sciences Analytiques, Université Pierre et Marie Curie, Bat. F, 4 Place Jussieu, 57252 Paris Cedex 05, France

ARTICLE INFO

Article history:
Received 27 September 2011
Received in revised form
12 December 2011
Accepted 13 December 2011
Available online 14 January 2012

Keywords:
Layered oxides
Intercalation compounds
Magnetic properties
Li-ion batteries

ABSTRACT

In this work, we studied the local environment of a series of $LiNi_yMn_yCo_{1-2y}O_2$ materials synthesized by wet chemistry via oxalate route. Measurements included the temperature dependence of the magnetic susceptibility $\chi_m(T)$, the magnetization $M(H)$, and the electron spin resonance. The influence of the synthesis conditions on the magnetic and electronic properties is presented and discussed. Magnetic properties and electron spin resonance spectroscopy provides further information on Ni^{2+}, Mn^{4+} ion distribution in $LiNi_yMn_yCo_{1-2y}O_2$. The magnetic data allows the determination of the cationic disorder, i.e. the concentration of Ni^{2+} ions in the 3*a* lithium sites, as a function of the composition, in quantitative agreement with the results of XRD experiments. We find that the lithium extraction proceeds by different steps. In a first step, Ni^{2+} in converted first in Ni^{3+}, then in Ni^{4+} as *x* decreases from $x=1$, while Co remains in the Co^{3+} valence state. The ESR spectra show a resonance due to Mn^{4+}, which is analyzed self-consistently with magnetic experiments.

1. Introduction

Layered oxide materials $LiMO_2$ ($M=3d$ transition metal elements) are among the most promising electrode materials for their applications in rechargeable Li-ion batteries [1–3]. These compounds have been exhibited with multiple transition-metal cations such as ($Ni_{0.8}Co_{0.2}$), ($Ni_{0.5}Mn_{0.5}$), ($Ni_{0.33}Mn_{0.33}Co_{0.33}O_2$) or more generally ($Ni_yMn_yCo_{1-2y}O_2$) with ultimate goals of large enhancement of the thermal and structural stability and appreciable increase of the capacity retention [4–8]. Recently, $LiNi_yMn_yCo_{1-2y}O_2$ materials were proposed to replace $LiCoO_2$, the most often used material in practical batteries [2]. The structure of layered $Li_xNi_yMn_yCo_{1-2y}O_2$ compounds consists of a cubic close-packed (*ccp*) arrangement of the oxide ions with the stacking sequence of *ABCABC* along the *c*-axis. The transition metal ions in the structure occupy alternating layers in the octahedral sites. Accordingly, these materials crystallize in the α-$NaFeO_2$ (O3-type) structure with the $R\bar{3}m$ symmetry. For an ideal $LiMO_2$ crystal, the ionic configuration is regulated with Li at the 3*a* site (0,0,0), *M* at the 3*b* site (0,0,1/2), and O at the 6*c* site (0,0,1/4) [9]. These compounds satisfy two rules. First, the sum of the cation occupations on the 3*b* sites of space group $R\bar{3}m$ in the transition-metal layers equals one. Second, the sum of the cation oxidation state times the cation occupation must equal three [10]. According to previous experiments (i.e. XANES, NMR, XPS) the oxidation states of Ni, Co, and Mn in these compounds are proved to be +2, +3, and +4, respectively [11–13].

Magnetic experiments are powerful tools to study fundamental properties and to check the quality of samples. Temperature, stress and impurities can all affect magnetic properties and play an important role in using materials for engineering applications. The estimation and analysis of the spontaneous magnetization can reveal ferromagnetic particles as impurities in the samples. The shape of the temperature dependence of the magnetization *M* measured in magnetic field $H=10$ kOe is indicative of the origin of the magnetic properties [14,15]. However, it is necessary to correlate the $\chi_m(T)=M/H$ curves and isothermal $M(H)$ plots to achieve a complete analysis of the electronic properties of the materials. For instance, it has been shown that $LiNiO_2$ grows with the presence of excess Ni ions randomly distributed at predominantly Li sites (3*a* Wyckoff position). The magnetic properties are extremely sensitive to the Ni^{2+} ion distribution and their analysis has been useful to evaluate the deviation *z* from stoichiometry in $Li_{1-z}Ni_{1+z}O_2$ [16]. For a review of the magnetic properties of lamellar compounds related to the present work, see [17].

In a previous work [18], we used tartaric acid as the chelating agent to prepare one element of this $Li_xNi_yMn_yCo_{1-2y}O_2$ series, corresponding to $x=1$, $y=1/3$. The purpose of this prior work was to report the efficiency of the combination of different techniques to characterize this compound, which allowed us to adjust the synthesis parameters (heating temperature, acid to metal-ion ratio) to obtain the 'optimized' sample, meaning optimize the crystallinity

* Corresponding author.
E-mail address: alain.mauger@impmc.jussieu.fr (A. Mauger).

0925-8388/$ – see front matter © 2011 Elsevier B.V. All rights reserved.
doi:10.1016/j.jallcom.2011.12.055

and reduce as much as possible the cationic disorder for this particular case $x = 1$, $y = 1/3$.

In the present work, we address the important question of current interest in the context of Li-ion batteries, namely which composition of the $LiNi_yMn_yCo_{1-2y}O_2$ series is most suitable to applications, in terms of stability and cationic disorder. For this purpose, we report the study of the local environment in the crystallographic structure of the whole series in the whole range $0.2 \leq 1-2y \leq 0.5$, and also at the different steps of delithiation $0 \leq x \leq 1$. In the following, the samples will be identified indifferently by their concentration y in Ni and Mn, or by their concentration $1-2y$ in cobalt when attention is focussed on the role played by this ion that is introduced to stabilize the lattice. The strategy we have adopted is the investigation of the magnetic properties, and we have added electron spin resonance (ESR) spectroscopy, since we found that the ESR resonance is quite sensitive to the cationic disorder. A different synthesis route has been chosen (the oxalic route), but the method of characterization is the same as in our prior work, so that the results are reported hereunder only for the 'optimized' samples. The results give a new insight on the role played respectively by the cobalt and the manganese on the chemical properties and stability of the lattice, and a new insight on the delithiation process. The self-consistent analysis of the different experimental properties gives for the first time quantitatively the evolution of the cationic disorder with the composition, and the evolution of the valence of the ions upon delithiation at the different steps x.

2. Experimental

The powders were prepared by wet chemistry using the oxalic acid assisted sol–gel method [19]. Stoichiometric amount of lithium acetate, $Li(CH_3COO)\cdot 2H_2O$, nickel acetate, $Ni(CH_3COO)_2\cdot 4H_2O$, manganese acetate, $Mn(CH_3COO)_2\cdot 4H_2O$, and cobalt acetate $Co(CH_3COO)_2\cdot 4H_2O$ (Alfa Aesar products) were dissolved in distilled water and mixed with aqueous solution of oxalic acid. The resulting solution was mixed with a magnetic stirrer at 80–90 °C for 6–8 h to obtain a clear viscous gel. The gel was dried in an oven at 140 °C for 12 h. The slurries were ground and pre-calcined at 400 °C for 24 h. The crystalline samples were formed by heating the precursor at 950 °C during 8 h in air.

XRD patterns have been recorded on a Philips X'Pert PRO MRD (PW3050) diffractometer equipped with a Cu anticathode (CuK_α radiation $\lambda = 1.54056$ Å) at room temperature. The measurements have been recorded under Bragg-Brentano geometry at 2θ with step 0.05° in the range 10–80°. SEM observations were realized by a high resolution electron microscope Hitachi (S-4700). The susceptibility and magnetization were measured using a superconducting quantum interference device (SQUID) magnetometer (Quantum Design MPMS). The derivative signals of the absorption ESR spectra have been recorded with the use of an X-band VARIAN spectrometer. The powder samples have been placed in an ESR Oxford Instruments continuous flow cryostat, allowing measurements in the whole temperature range between room temperature and 3.5 K. The cryostat itself was inserted in a TE 102 microwave cavity. The frequency of the microwave field was 9.25 GHz. The frequency of the *ac* modulation magnetic field was 100 kHz, and the *dc* magnetic field varied in the range 0–20 kOe. FTIR absorption spectra were recorded with a Fourier transform interferometer (model Bruker IFS113 v) in the wavenumber range 150–1400 cm^{-1} at a spectral resolution of 2 cm^{-1}. The samples were ground to fine powders and dispersed into a CsI pellet in the proportion (1:300).

The lithium extraction from $LiNi_yMn_yCo_{1-2y}O_2$ powders was made by chemical delithiation using molar fraction of potassium peroxydisulfate ($K_2S_2O_8$) in an aqueous solution. The molar ratios $LiNi_yMn_yCo_{1-2y}O_2$:$K_2S_2O_8$ were 4:1 and 2:1 to obtain $LiNi_yMn_yCo_{1-2y}O_2$ with $x = 0.5$ and $x = 0$ samples, respectively. The mixture $LiNi_yMn_yCo_{1-2y}O_2$ and $K_2S_2O_8$ dissolved in water was stirred at room temperature for 24 h. The powders were washed, filtered and dried at 800 °C.

Li, Co, Ni, and Mn contents (with an error of 3%) in the resulting materials were analyzed using an inductively coupled plasma/atomic emission spectrometer (ICP/AES, Kontron S-35). The obtained mole ratios were calculated from the average weight-percent of three repeated ICP-data of each analyzed element. The results are reported in Table 1 for some of the samples investigated before delithiation. The Li concentration x upon delithiation was also verified by ICP and XRD measurements. Both methods gave the same values.

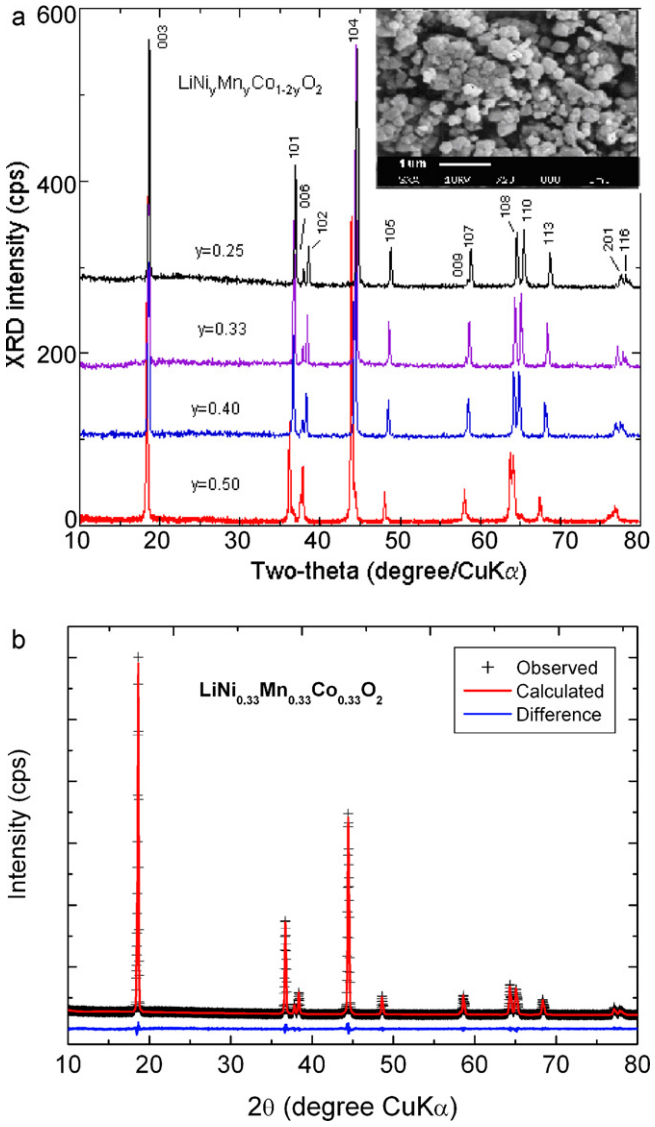

Fig. 1. XRD pattern of $LiNi_yMn_yCo_{1-2y}O_2$ ($0.0 \leq 1-2y \leq 0.5$) materials synthesized by wet-chemistry via oxalate route (a). Bragg lines have been indexed in the rhombohedral system ($R\bar{3}m$ S.G.). Insert presents the SEM image of the $y = 1-2y = 1/3$ sample post-treated at 950 °C for 8 h. (b) shows the Rietveld refinement for one of the samples.

3. Results

3.1. Structural characterization

XRD patterns of the synthesized powders, $LiNi_yMn_yCo_{1-2y}O_2$, are shown in Fig. 1a for various compositions. The insert in the figure is the SEM image of our samples. The Rietveld refinement is illustrated for one of them in Fig. 1b. The samples in the whole range of compositions are single phase with rhombohedral structure of α-$NaFeO_2$-type ($R\bar{3}m$ space group) similar to the high temperature polymorph of $LiCoO_2$ [9]. The electron diffraction patterns exhibit the good crystallinity of $LiNi_yMn_yCo_{1-2y}O_2$ powders. Lattice parameters of powders fired at 950 °C in air are listed in Table 2. We have shown elsewhere how the Rietveld analysis of the XRD spectra can be used to determine the site-exchange ratio of Li^+ and Ni^{2+} ions [20,21]. The same analysis in the present work shows that this ratio decreases from 6.7% to 0.7% upon increasing the Co concentration. This is the first benefit of the substitution of Co for Mn. The c/a ratio of the lattice constants is a direct measure of the

Table 1
The elemental analysis of the $Li_xNi_yMn_yCo_{1-2y}O_2$ ($0.2 \le 1-2y \le 0.5$) powders by the ICP method.

Sample	Element in wt.% [mole ratio]			
	Li	Co	Ni	Mn
$LiCoO_2$	6.98 [1.005]	58.81 [0.998]	–	–
$LiNi_{0.4}Mn_{0.4}Co_{0.2}O_2$	6.91 [0.995]	12.43 [0.211]	23.19 [0.395]	21.48 [0.391]
$LiNi_{0.33}Mn_{0.33}Co_{0.33}O_2$	7.01 [1.010]	19.44 [0.330]	19.07 [0.325]	18.69 [0.340]
$LiNi_{0.3}Mn_{0.3}Co_{0.4}O_2$	6.95 [1.002]	23.86 [0.405]	17.90 [0.305]	16.37 [0.298]
$LiNi_{0.25}Mn_{0.25}Co_{0.5}O_2$	6.92 [0.997]	29.17 [0.495]	14.38 [0.245]	13.89 [0.253]

Table 2
Lattice parameters of $LiNi_yMn_yCo_{1-2y}O_2$ ($0.25 \le y \le 0.5$) powders deduced from Rietveld refinements.

Co content $(1-2y)$	a (Å)	c (Å)	c/a	η (%)
0.00	2.9033 (2)	14.365 (2)	4.948	6.7
0.20	2.8745 (1)	14.267 (8)	4.963	5.0
0.33	2.8646 (3)	14.291 (2)	4.977	2.8
0.40	2.8586 (5)	14.239 (1)	4.981	1.4
0.50	2.8517 (1)	14.219 (6)	4.986	0.7

deviation of the lattice from the perfect cubic closest packing (*ccp*). The trigonal distortion leading to c/a larger than the *ccp* value 4.899 indicates that the substitution of Co for Mn in $LiNi_yMn_yCo_{1-2y}O_2$ also promotes the formation of the layered structure.

The investigated samples have complex compositions and are prepared from the metal acetate hydrates. The starting materials normally vary with respect to their specific hydrate content. This effect could falsify the metal ratios in the educt mixture and consequently also in the product. Therefore, an independent check of the water content of the educts is desirable, although the ICP results in Table 1 show that the metal ratios in the final product is in quantitative agreement with the expectation value. For this purpose, TGA experiments have been done. The results are illustrated in the insert of Fig. 2, starting form the initial mixture for the $LiNi_{0.33}Mn_{0.33}Co_{0.33}O_2$ sample, chosen as an example. First, a smooth and continuous loss of weight is observed as the temperature increases up to 250 °C (marked by the letter A in the figure). Heating above this temperature results in a sharp decrease of weight, and the weight is stabilized above 700 °C, up to the temperature 950 °C used for the preparation of the samples (marked by the letter B in the figure). To understand theses results, FTIR spectra are shown in Fig. 2 at these two temperatures 250 °C and 950 C. Below 1000 cm^{-1}, the spectra show the characteristic bands associated with the internal vibration modes of $Li_xNi_yMn_yCo_{1-2y}O_2$. Therefore, the final product is already forming at 250 °C. Nevertheless, the bands are quite broad, which gives evidence that we are experiencing the first step of the synthesis. This is at contrast with the spectrum at 950 °C, in which the intrinsic bands are narrow, the evidence that the material is now well crystallized. Additional bands are observed on the spectrum at 250 °C. The two bands at circa 1420 cm^{-1} and 1730 cm^{-1} are attributable to C–H bending [22] and ν(C=O) [23], respectively. The presence of these vibrations due to the organic precursors gives another evidence that all the acetate hydrates are not fully decomposed at this temperature. The two other bands in the range 2800–3000 cm^{-1} are attributable to ν(OH) vibrations [22]. All these vibrations have disappeared in the spectrum at 950 °C. Therefore, the samples are free of any structural water and of any hydrates and organic compound, and actually, heating at 700 °C is sufficient to get rid of all these products, as no loss of weight is observed in TGA results above 700 °C. Heating at 950 °C was needed simply to improve the crystallinity.

3.2. Magnetic properties of $LiNi_yMn_yCo_{1-2y}O_2$ ($0.2 \le 1-2y \le 0.5$)

The magnetization curves $M(H)$ at different temperatures have been measured for different compositions y. The result is illustrated for $y = 0.4$ in Fig. 3. A spin freezing is observed, characterized by the onset of a remanent magnetization at the temperature Tc, reported in Table 3, for the various compositions investigated. The temperature dependence of the reciprocal magnetic susceptibility, χ_m^{-1}, is shown in Fig. 4 for all samples. In these experiments, χ_m is defined as M/H measured in applied magnetic field $H = 10$ kOe. We have shown earlier that Tc is associated to a spin freezing of ferromagnetic clusters of finite size [20,21]. We shall recall the origin of this magnetic clustering hereunder. For the moment, we simply note that the dynamics of such a transition are known to be slow at low magnetic field, leading to a difference between FC and ZFC magnetic

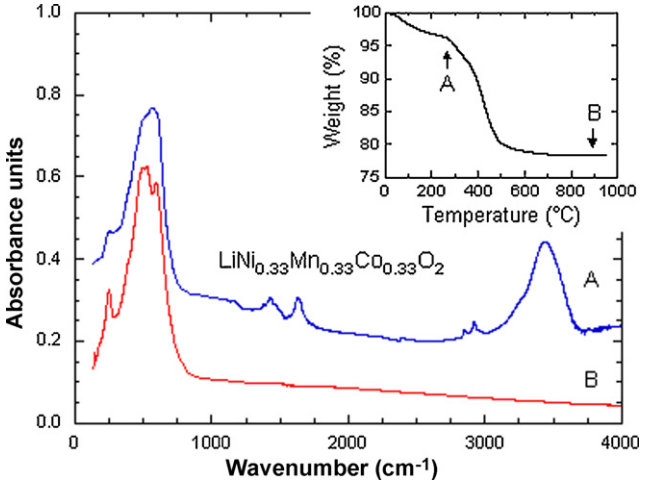

Fig. 2. FTIR spectra of the $LiNi_{0.33}Mn_{0.33}Co_{0.33}O_2$ sample at 250 and 950 °C, labeled A and B, respectively. The TGA experiment is shown in insert.

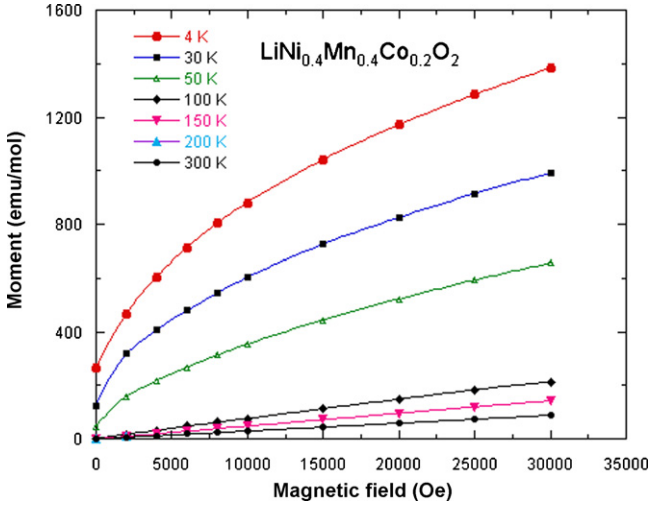

Fig. 3. Isothermal plots of the magnetization $M(H)$ for $LiNi_{0.4}Mn_{0.4}Co_{0.2}O_2$ powders synthesized via the oxalate route.

Table 3
Magnetic parameters of $LiNi_yMn_yCo_{1-2y}O_2$ ($0.2 \le 1-2y \le 0.5$).

$1-2y$(Co)	Tc (K)	θ_p (K)	μ_{eff} experimental	μ_{eff} theoretical (μ_B)	% Ni^{2+} in 3a site
0.5	8	−90	2.44	2.40	0.7
0.33	30	−103	2.84	2.75	3.0
0.2	60	−93	3.05	3.03	5.0
0.0	140	−87	3.25	3.39	7.0

susceptibilities. These dynamics, however, are accelerated by application of an external magnetic field. The applied field $H = 10$ kOe has been chosen high enough so that the FC and ZFC magnetic susceptibilities cannot be distinguished from each other in our experiments, so that χ_m is defined unambiguously. In counterpart, this value of H is large enough to smear out the transition, so that Tc corresponds to a simple inflexion point in the χ_m^{-1}(T) curves. We can find in Fig. 4 a high temperature regime where χ_m^{-1}(T) is linear, which is also the regime where M is linear in H, as it can be seen in Fig. 3 for the composition chosen to illustrate the magnetization curves. This concomitant feature gives evidence that the mean field approximation neglecting the spin correlations is valid in this temperature range, so that the Curie–Weiss law $\chi_m^{-1} = (T-\theta_p)/C_p$ applies. The Curie constant C_p and the paramagnetic Curie–Weiss temperature θ_p are reported in Table 3 for the different samples. The cobalt is trivalent in the material, and Co^{3+} is a non-magnetic ion in its low spin-state ($S = 0$). Neglecting its very small contribution to the magnetization, we can consider that only Mn and Ni contribute to χ_m. It is well established that these ions are in the Mn^{4+} and Ni^{2+} configurations in these compounds and that their orbital moment is quenched by the crystal field [11,13,17,21–24], so that their effective magnetic moment is their spin-only value, namely $3.87\mu_B$ and $2.83\mu_B$, for Mn^{4+} and Ni^{2+}, respectively. Indeed, we find that the theoretical effective moment $\mu_{eff} = [y(2.83)^2 + y(3.87)^2]^{1/2}\mu_B$ is in good agreement with the experimental value deduced from the Curie constant C_p for all the values of y investigated, at it can be seen in Table 3.

According to the layered structure of the lattice, the metal ions occupy layers of octahedral interstitials between cubic close-packed arrays to form O–(Mn^{4+}, Ni^{2+}, Co^{3+})–O sandwiches. The dominant magnetic interactions between the magnetic ions for the intrinsic compound are then intra-layer superexchange

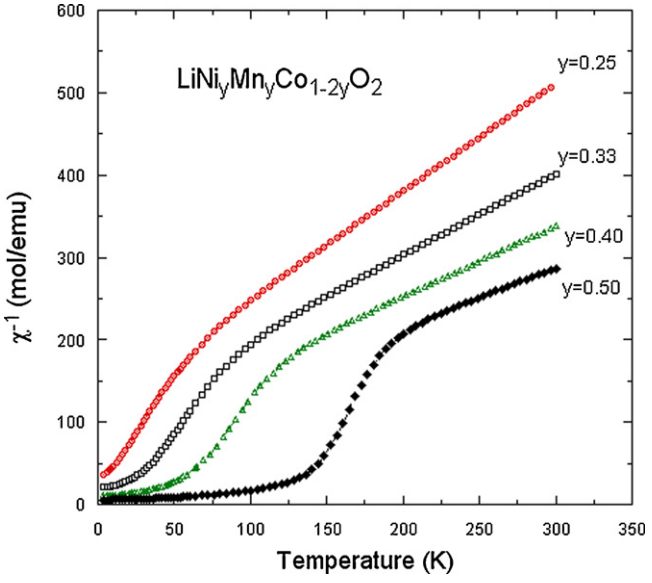

Fig. 4. Plot of the magnetic susceptibility H/M for $LiNi_yMn_yCo_{1-2y}O_2$ ($0.0 \le 1-2y \le 0.5$) samples prepared by wet chemistry assisted by oxalic acids.

interactions mediated via the oxygen inside this sandwich at 90° bonding angle. These magnetic interactions have been studied in prior works, and are a mixture of ferromagnetic (FM) and antiferromagnetic (AFM) interactions [25,26]. The large and negative value of θ_p, however, reveals that AFM interactions are dominant, so that FM ordering of the bulk material in this case is not expected. We have argued in previous studies [20,27] that the ferromagnetism is extrinsic in nature. Following our prior works [20,25] we identify the fraction of magnetic ions contributing to the extrinsic ferromagnetism to Ni^{2+} ions that occupy the 3a Wyckoff site of the lithium sublattice and generate 180° interlayer Mn^{4+}(3b)–O–Ni^{2+}(3a) ferromagnetic interactions after the Goodenough rules [28]. When attributing the remanent magnetic moment at low temperature to the magnetic moment at saturation of Mn^{4+}(3b)–Ni^{2+}(3a) pairs spin-frozen in a ferromagnetic order, we have found a concentration of Ni^{2+}(3a) defects in quantitative agreement with the result deduced from the Rietveld refinement of the XRD spectra in $Ni_{1/3}Mn_{1/3}Co_{1/3}O_2$ (i.e. $y = 1/3$) [20,21,24]. We also found 7% of Ni^{2+}(3a) impurities in $LiNi_{0.5}Mn_{0.5}O_2$ [20] which compares well with the results of the structural analysis by X-ray diffraction [29], synchrotron and neutron diffraction experiments [30] on different samples of the same composition $y = 1/2$. We then follow the same analysis in the present case. The remanent magnetization at $T = 4$ K is in the order of 50, 250, and 600 emu/mol for $(1-2y) = 0.5$, 0.33, and 0.2 respectively. The corresponding concentration of Ni^{2+}(3a) defects is reported in Table 3. In all cases, we also find a quantitative agreement with the concentration of Ni^{2+}(3a) defects deduced from the Rietveld refinement of the XRD spectra (see Table 2).

In the layered system investigated here, the almost linear Ni^{2+}(3a)–O–Mn^{4+}(3b) magnetic path leads to a ferromagnetic interaction that is stronger than the AFM interactions above mentioned responsible for a negative paramagnetic Curie temperature. Therefore these AFM interactions cannot prevent the ferromagnetic freezing of the Ni^{2+}(3a)–O–Mn^{4+}(3b) locally near the Ni^{2+}(3a) defect. However, they prevent the material from a cooperative ferromagnetic ordering at a Curie temperature below which all the Mn^{4+} and Ni^{2+} ions would align their magnetic moment, simply because such an ordering supposes a concentration of ferromagnetic pairs at least equal to the critical concentration for the percolation transition [31], and the amount of Ni^{2+}(3a) defects estimated in the material (Tables 2 and 3) is at least three times smaller than the percolation threshold for a two-dimensional lattice. Therefore, Tc in our material is not a Curie temperature that is associated to the cooperative long-range ferromagnetic ordering. It is simply defined as the temperature that characterizes the onset of a remanent magnetization associated to the spin freezing of the Mn^{4+}(3b)–Ni^{2+}(3a) ferromagnetic pairs diluted in the matrix.

The fraction of Ni^{2+}(3a) displayed in Table 3 for the samples $1-2y \neq 0$ investigated in the present work decreases with the

Table 4
Magnetic parameters of delithated $Li_xNi_yMn_yCo_{1-2y}O_2$.

Co content ($1-2y$)	Tc (K)	θ_p (K)	μ_{eff} (μ_B) experimental	x
0.50	8	−210	3.04	0.52
0.33	30	−254	3.90	0.27
0.00	140	−201	4.22	0

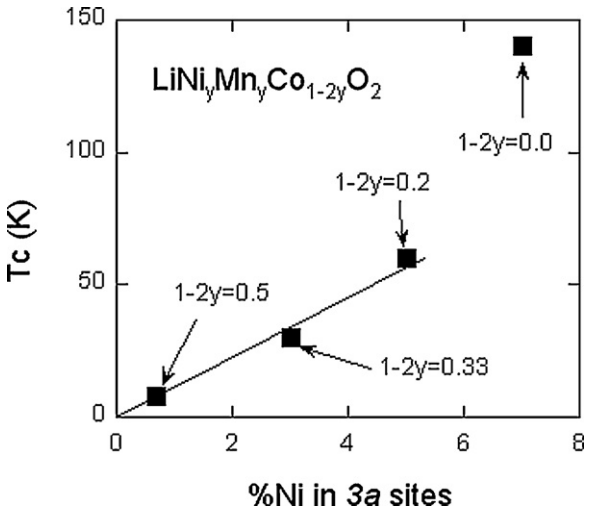

Fig. 5. Temperature *Tc* defined by the onset of a remanent magnetization as a function of the concentration of $Ni^{2+}(3a)$ defects. The straight line is theoretical, after Eq. (1).

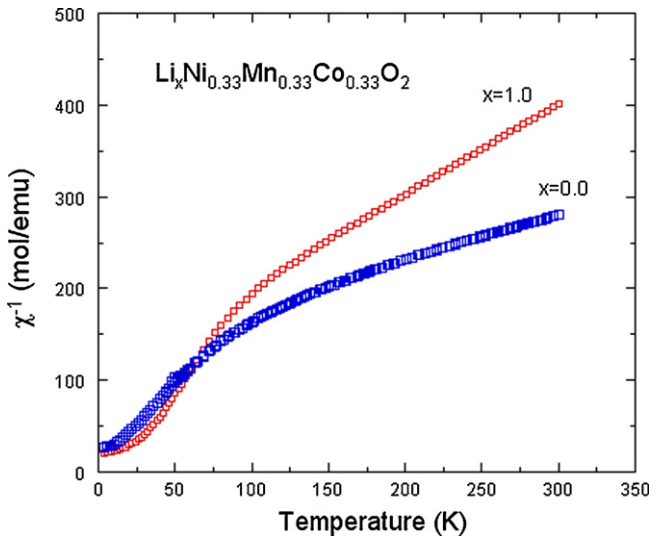

Fig. 6. Temperature dependence of the reciprocal magnetic susceptibility of $Li_xNi_{0.33}Mn_{0.33}Co_{0.33}O_2$ materials for $x = 1$ and $x = 0.27$. The $Li_xNi_{0.33}Mn_{0.33}Co_{0.33}O_2$ sample was prepared by chemical delithiation using the potassium peroxydisulfate method.

amount of cobalt. This is actually expected, if we remember that the introduction of cobalt aimed at stabilizing the lattice and, indeed, this stabilization reflects in the decrease of $Ni^{2+}(3a)$ native defects. In a diluted magnetic semiconductor, defined as an assembly of localized spins *S* in concentration *c* diluted on the lattice sites of a semiconductor matrix, *Tc* can be evaluated in the mean field approximation, as

$$Tc = c\frac{4S(S+1){\mu_B}^2}{3k_B}J(q=0), \quad (1)$$

where k_B is the Boltzmann constant, and $J(q)$ is the Fourier transform of the exchange interaction at the vector $q = 0$ averaged over the disorder [32]. We are in the same situation here, with *S* the effective spin associated to the $Ni^{2+}(3a)$–$Mn^{4+}(3b)$ ferromagnetic pairs. The variation of *Tc* with the concentration $c = [Ni^{2+}(3a)]$ of nickel on $(3a)$ sites is reported in Fig. 5. Indeed we find that the linear law $Tc \propto [Ni^{2+}(3a)]$ according to Eq. (1) is well satisfied, except for the sample without any cobalt where the concentration of such defects is too large and thus located outside the linear regime. The same behavior has been observed in other spin-diluted semiconductors [32–34].

3.3. Magnetic properties of delithiated $Li_xNi_yMn_yCo_{1-2y}O_2$

Fig. 6 illustrates the temperature dependence of the reciprocal magnetic susceptibility of $Li_xNi_yMn_yCo_{1-2y}O_2$ delithiated sample for one Co concentration chosen as an example $(1 - 2y = 0.33)$ for $x = 0.27$, together with the same curve obtained before delithiation $(x = 1)$ for comparison. We shall detail hereunder how this composition $x = 0.27$ has been determined. The main effect is in the paramagnetic regime where the Curie constant has been changed, because the valence of the magnetic ions has changed. The effective moment μ_{eff} deduced from the slope of the H/M curves in the paramagnetic regime where the Curie–Weiss law is satisfied is reported for the different samples in Table 4. We find, however, that μ_{eff} deviates from the theoretical value predicted for full delithiation that would be achieved if the transition ions were in the Ni^{4+}, Mn^{4+}, and Co^{4+} valence state. This deviation gives evidence that we could not remove completely the lithium in these samples. Since, however, the limit $x = 0$ could be reached in absence of cobalt [20], the limit in the delithiation process comes from the difficulty to change the oxidation state of Co from Co^{3+} to Co^{4+}. We find that the delithiation proceeds by different steps. In a first step, Ni^{2+} in converted first in Ni^{3+}, then in Ni^{4+} as *x* decreases from $x = 1$, while Co remains in the Co^{3+} valence state. As more Li^+ ions are removed, we reach a situation where no Ni^{2+} remains (besides the Ni ions on the $(3a)$ sites, but in samples with Co in them, Ni$(3a)$ defects are in so small concentration that they we can neglect them for this purpose). Basically, we can pursue the delithiation process up to the point where more or less all the Ni^{2+} will be converted in Ni^{4+} In case some Ni^{3+} ions remain, we can write the chemical formula of the samples $Li^+_xNi^{3+}_{y'}Ni^{4+}_{y-y'}Mn^{4+}_yCo^{3+}_{1-2y}O^{2-}_2$. Then the equation of neutrality of electronic charge is

$$x = 1 + y' - 2y \quad (2)$$

The theoretical value of the effective magnetic moment μ_{eff} entering the Curie constant in the paramagnetic regime can be determined, taking into account the spins carried by the magnetic ions. We know from earlier works [20,35,36] that Ni^{3+} ions is in the low spin state (spin $S = 1/2$) and Ni^{4+} is in the high spin state $(S = 2)$ in the materials of this family. Therefore, μ_{eff} is:

$$\mu_{eff} = [3y' + 24(y - y') + 15y]^{1/2} \quad (3)$$

The first term in the second member of Eq. (3) is the contribution from the Ni^{3+} ions, the second term is that of Ni^{4+}, while the third term is that of Mn^{4+} (spin $S = 3/2$). The comparison between the experimental value of the effective magnetic moment and this formula in Eq. (3) allows us to determine the value of y'; then *x* can be determined from Eq. (2). An example of this situation is provided for the sample with the cobalt concentration $1 - 2y = 0.5$ for which the Li content determined by this procedure is $x = 0.52$. Note we find $y' = 0.02$ in this sample. This very small concentration of Ni^{3+} ions is comparable with the uncertainty in the determination of this parameter, so that this result means essentially that all the nickel has been converted in Ni^{4+} in this sample. Note also that the magnetic measurements show unambiguously that the Ni^{4+} is in the high spin state. This is actually imposed by the strong magnetic moment μ_{eff} observed in our samples. For instance, taking again the example $1 - 2y = 0.5$, the value of y' that would be the solution of Eq. (3) in case Ni^{+4} would be in the low spin $(S = 0)$ state according to the experimental value of μ_{eff} would be $y' = 2$, which is non-physical since this parameter is submitted to the constraint $y' \leq y$.

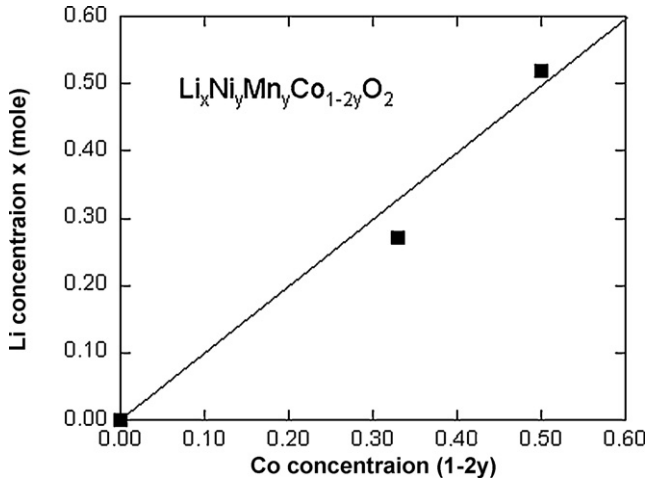

Fig. 7. Composition x of the samples $Li_xNi_yMn_yCo_{1-2y}O_2$ after delithiation, as a function of the cobalt concentration. The full line corresponds to the situation where all the nickel ions are tetravalent, and all the cobalt ions have remained in the trivalent state.

Upon further delithiation, we may reach a situation where all the Ni ions are converted into Ni^{4+} ions, and finally even a part of Co^{3+} is converted into Co^{4+}, so that we can write the chemical formula of the samples $Li^+{}_xNi^{4+}{}_yMn^{4+}{}_yCo^{3+}{}_{1-2z}Co^{4+}{}_{2z-2y}O^{2-}{}_2$. Then Eqs. (2)–(3) must be replaced by

$$x = 1 - 2z \tag{4}$$

$$\mu_{eff} = \mu_B[15y + 24y + 70(z - y)]^{1/2} \tag{5}$$

The last term in Eq. (5) comes from the Co^{4+} ion which carries a spin $S = 5/2$ in the high spin state. This situation is illustrated for the sample with the Co content $1 - 2y = 0.33$, for which we find $x = 0.27$. Note that we find a concentration of Co^{4+} that is $2(z - y) = 0.067$. This is actually not negligible, but small, emphasizing again the difficulty we met in changing the valence of the cobalt. This feature is expected since the chemical process used in the present work is known to be a soft process to delithiate the sample, making very difficult the oxidation of the cobalt [37]. Again the magnetic measurements show unambiguously that the Co^{4+} ion is in the high spin state: for the case $1 - 2y = 0.33$ illustrated in the figure, the solution of Eq. (5) if the Co^{4+} ions were in the low-spin state taking the experimental value of μ_{eff} into account would be $2(z - y) = 1.67$, an unphysical solution since the chemical formula requires $z \leq 1/2$. Therefore, there is only one unique physical solution to the Eqs. (2)–(5), which gives evidence that the magnetic ions in the tetravalent valence state are all in the high-spin state in these lamellar compounds. In the case of Ni^{4+}, the result was already known [20,35,36], but in the case of Co^{4+} the result is not trivial since Co^{4+} is in the high-spin state in Li_xCoO_2 for $0.94 < x < 1.00$, and low-spin state for $0.50 < x < 0.78$ [38,39]. We shall return to this feature in the discussion.

The situation where exactly all the Ni^{2+} has been converted in Ni^{4+} while the cobalt has remained in the trivalent state corresponds to the particular case $y' = 0$ in Eq. (2) or $z = y$ in Eq. (4), namely

$$x = 1 - 2y. \tag{6}$$

This linear behavior, compared with the results for the delithiation of our samples is illustrated in Fig. 7. Just as in the case of the sample without cobalt $(1 - 2y) = 0$ we have investigated in an earlier work [20], we find that the magnetic susceptibility does not much depend on x below Tc, i.e. in the temperature range where the magnetic susceptibility is dominated by the ferromagnetic spin freezing. It shows unambiguously that neither

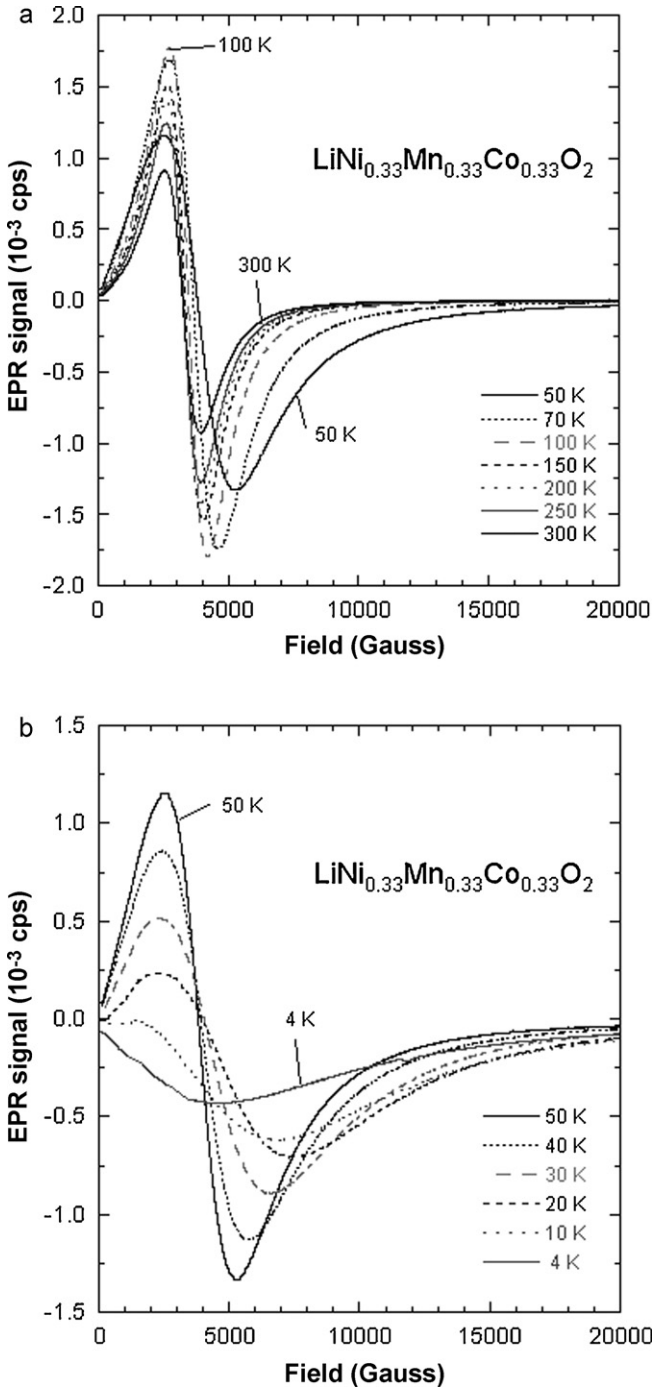

Fig. 8. Electron spin resonance spectra of $LiNi_{0.33}Mn_{0.33}Co_{0.33}O_2$ at different temperatures: (a) above Tc and (b) below Tc. The spectrum at 50 K is reported both in (a) and (b) to follow the evolution in temperature.

the $Mn^{4+}(3b)$–$Ni^{2+}(3b)$ nor the $Ni^{2+}(3b)$–$Ni^{2+}(3b)$ magnetic interactions play any role in the ferromagnetic spin freezing observed at Tc in the $LiNi_yMn_yCo_{1-2y}O_2$, since there is essentially no $Ni^{2+}(3b)$ left after delithiation.

3.4. ESR spectra of $LiNi_yMn_yCo_{1-2y}O_2$ $(0.2 \leq 1 - 2y \leq 0.5)$

The electron paramagnetic resonance of $LiNi_yMn_yCo_{1-2y}O_2$ has been measured at different temperatures for different compositions. The result is illustrated for two of them in Figs. 8 and 9. Ni^{2+} has an integer spin $S = 1$, which is not favorable to the observation

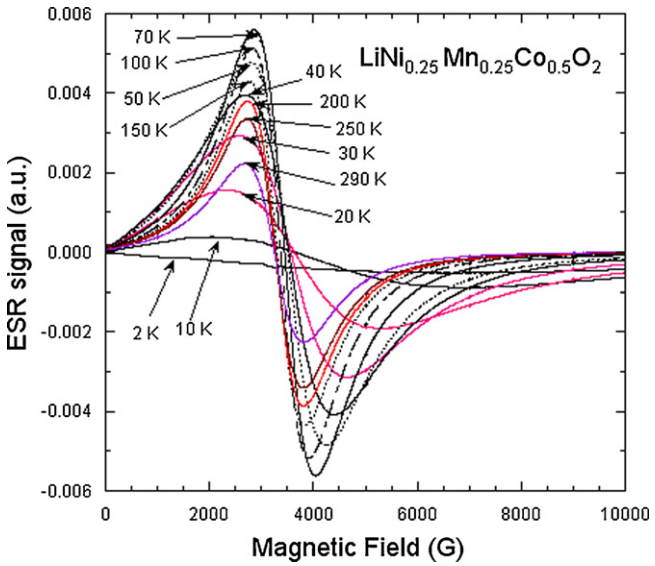

Fig. 9. Electron spin resonance spectra of $LiNi_{0.25}Mn_{0.25}Co_{0.50}O_2$ at different temperatures.

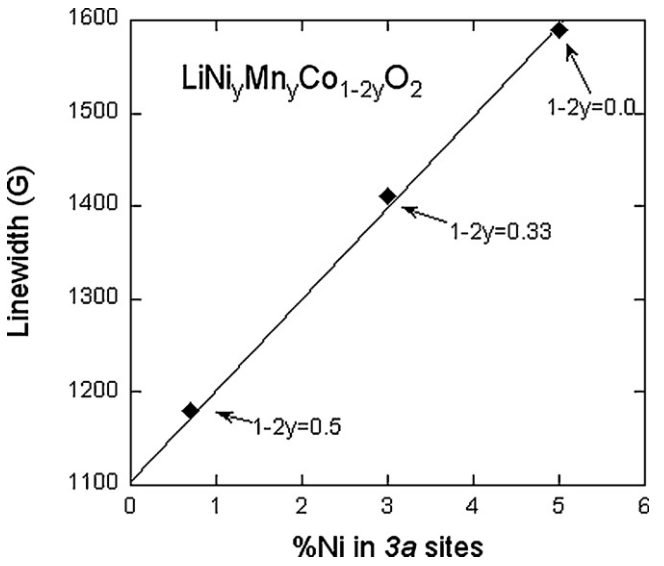

Fig. 11. Linewidth of the ESR line of $LiNi_yMn_yCo_{1-2y}O_2$ as a function of the $Ni^{2+}(3a)$ defect concentration.

of the ESR signal. An ESR signal associated to Ni^{2+} impurities can be detected in some materials when the amount of Ni^{2+} is the order of the % [37]. However, when the amount of Ni^{2+} ions is large as it is in the present case, the signal is broaden by local strains, so that no ESR signal associated to this ion can be detected. The lack of an EPR signal at X-band frequency for octahedral Ni^{2+} with a $^3A_{2g}$ ground term can also arise because the zero-field splitting in the electron spin triplet is very large relative to the microwave energy, and hence resonances are outside the available field range of the electromagnet. The paramagnetic resonance detected is attributable to the presence of Mn^{4+} ions that carry a half-integer spin ($S = 3/2$) and are then ESR-active. The position of the center of the signal is close to 3200 G. This is the position expected for uncorrelated spins with the gyromagnetic factor $g = 2.0$, for the microwave frequency we have used. The linewidth ΔB is small at room temperature, namely 1580, 1410 and 1150 G for $(1-2y) = 0.2$, 0.33 and 0.5 respectively, and varies very little with the temperature in the paramagnetic phase, as it can be seen in Fig. 10. On another hand, there is a strong broadening

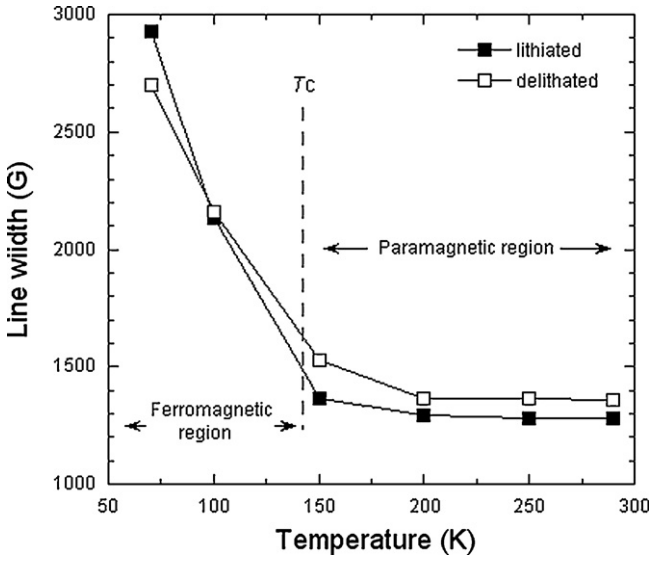

Fig. 10. Temperature dependence of the linewidth of the ESR line in $LiNi_yMn_yCo_{1-2y}O_2$.

of the line upon cooling below *Tc*, so that *Tc* is evidenced in Fig. 10 by the change in the slope of $\Delta B(T)$. This increase of $\Delta B(T)$ below *Tc* is due to the partial spin freezing in the ferromagnetic domains evidenced by the presence of a finite remanent magnetization. In addition, the line shape below *Tc* is no longer Lorentzian, as it can be seen in Fig. 10b. This change in the line shape can be already detected above *Tc* in Fig. 10a, namely in the range $Tc < T < 100$ K where short-range ferromagnetic spin interactions take place as a pre-transitional effect of the onset or the ferromagnetic clusters at *Tc*. Such spin correlations are responsible for the positive curvature of the $\Delta B(T)$ curve in Fig. 10 in this temperature range. In the ESR spectra, they also modify the line shape since the negative part of the ESR signal extends progressively at much larger magnetic fields. An important feature, however, is the fact that the linewidth still increases upon cooling even at temperatures twice smaller than *Tc*. This gives evidence that the Mn^{4+} spins are not frozen even at such low temperatures. This is fully consistent with the analysis of the direct magnetic measurements in the previous section, which has shown that only a small fraction of the Mn^{4+} spins are frozen in a ferromagnetic state.

The ESR linewidth ΔB for $LiNi_yMn_yCo_{1-2y}O_2$ oxides decreases as the Co amount increases, as it can be seen in Fig. 11. A decrease of $\Delta B(T = 300\,K)$ upon dilution of the magnetic ions (Co^{3+} is non-magnetic) is expected. However, the dilution rate $(1-2y) \leq 0.5$ remains smaller than the percolation threshold for the magnetic ions sublattice, while magnetic dilution effects should be important beyond this percolation threshold. The large and quasi-linear variation of ΔB with the Co-content is then more likely attributable to the decrease of the concentration of $Ni^{2+}(3a)$ impurities and the ferromagnetic spin interactions associated with them, upon increasing the Co content. $\Delta B(T = 300\,K)$ in Fig. 11 varies roughly linearly as a function of the concentration of $Ni^{2+}(3a)$ impurities, so that it can be extrapolated to determine the intrinsic limit, i.e. the value of ΔB in absence of $Ni^{2+}(3a)$ impurities. The result is 1100 G.

3.5. ESR spectra of the delithiated phases

The ESR spectra for the delithiated $Li_xNi_yMn_yCo_{1-2y}O_2$ samples are illustrated in Figs. 12 and 13 for the samples the ESR spectra of which is illustrated before delithiation in Figs. 8 and 9. The units are arbitrary, but they are the same in Figs. 8, 9 and 12, 13 allowing for a direct comparison between the spectra. Since the spectra of

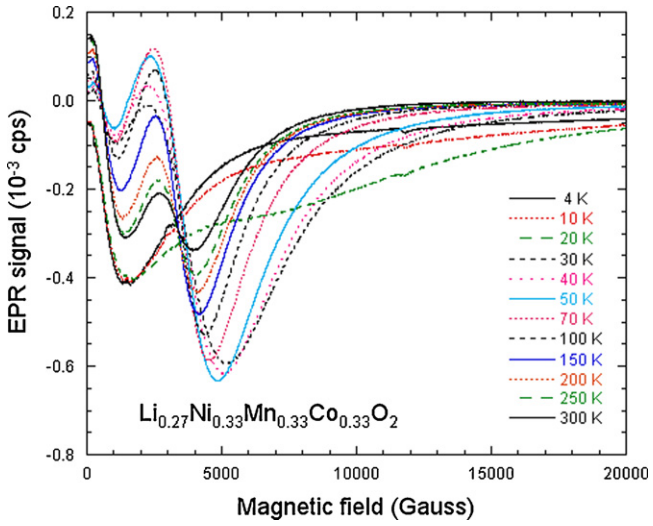

Fig. 12. Electron spin resonance spectra of $Li_{0.27}Ni_{0.33}Mn_{0.33}Co_{0.33}O_2$ at different temperatures.

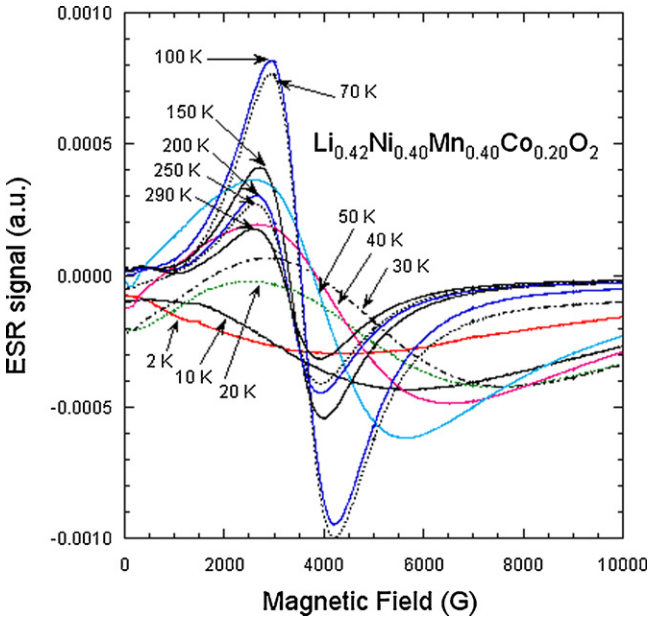

Fig. 14. Electron spin resonance spectra of $Li_{0.42}Ni_{0.40}Mn_{0.40}Co_{0.20}O_2$ at different temperatures.

delithiated samples are quite different from the $x = 1$ case, when x is so small that part of the cobalt ions are in the Co^{4+} valence state, which is the case in Figs. 12 and 13, we also investigated the ESR spectra of samples with an intermediate Li concentration to follow the modifications of the spectra more continuously as a function of x. The result is illustrated in Fig. 14 that shows the ESR spectrum of $Li_{0.42}Ni_{0.4}Mn_{0.4}Co_{0.20}O_2$. The Li concentration has been determined as explained in the section devoted to the magnetic properties, i.e. from the effective magnetic moment. This partial delithiation corresponds to a situation described in the formula $Li^{+}_{0.42}Ni^{3+}_{0.22}Ni^{4+}_{0.18}Mn^{4+}_{0.40}Co^{3+}_{0.20}O^{2-}_{2}$. The delithiation has been stopped at a stage where both Ni^{3+} and Ni^{4+} still exist in the same proportion, which guarantees the absence of Co^{4+} after the discussion of the previous section. We have argued in the previous sections that the main effect of the delithiation on the transition metal ions is to change Ni^{2+} in Ni^{3+} and Ni^{4+}. However, Ni^{2+} is not detected in the ESR spectra for reasons already mentioned, and Ni^{4+} is not detectable either. The reason is that the Ni^{4+} ions have an important orbital momentum, so that they are strongly coupled to the lattice by the crystal field. This strong crystal field coupling is responsible for such a broadening of the ESR signal associated to Ni^{4+} that it could not be detected. Note Ni^{4+} has the same electronic configuration as Fe^{2+}, and for the same reason no ESR signal associated to this ion can be detected in stoichiometric $LiFePO_4$ for instance [37]. Ni^{3+} is a Jahn-Teller ion, and as such is hardly detected by ESR, since it is very sensitive to the local strains that modify its ground state, unless the Ni^{3+} concentration is the order of the %. Actually, the integrated ESR signal in our samples is the same before and after delithiation, despite the fact that the Ni^{3+} concentration has strongly increased in the delithiation process. This gives evidence that the ESR signal in Fig. 14 is not related to Ni^{3+}; it is the EPR signal of Mn^{4+} ions, the concentration of which has not been modified in the delithiation process. For the same reason, this line is still centered at 3200 G. The only sizeable effect of the delithiation for this ESR line associated to Mn^{4+} is an increase of ΔB at given temperature. The change in the Coulomb interactions between ions upon delithiation may induce microstrains at the origin of this broadening of the linewidth in the delithiated samples. Some authors have claimed the observation of an ESR signal associated to Ni^{3+} in $LiNi_yCo_{1-y}O_2$ [40], although the observation of this signal is not expected in that case for reasons recalled above. Our results on similar lamellar compounds in the present work, which show the lack of any EPR signal associated Ni^{3+} suggest that the analysis of the EPR spectra in Ref. [40] should be revisited: the signal attributed to Ni^{3+} might be attributable to impurities, especially as the intensity of the EPR line has not been correlated to the Ni-content; moreover ΔB does not scale with y.

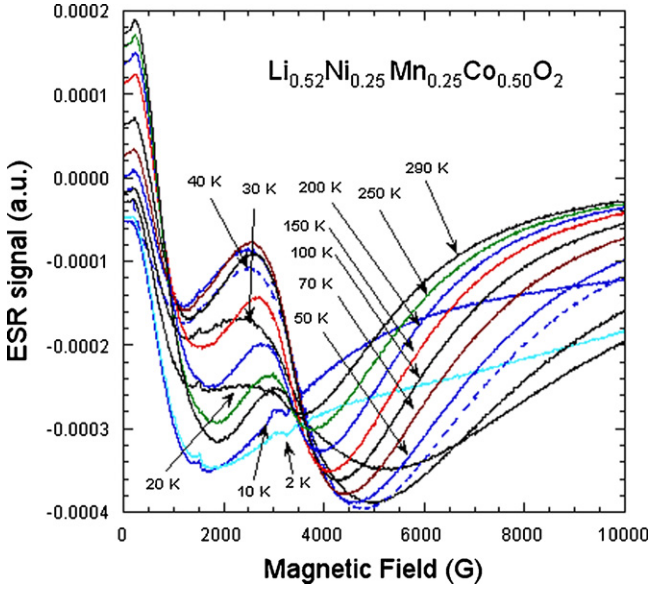

Fig. 13. Electron spin resonance spectra of $Li_{0.52}Ni_{0.25}Mn_{0.25}Co_{0.50}O_2$ at different temperatures.

Another structure at lower field is observed in the ESR spectra shown in Figs. 12 and 13, which should then be related to the existence of Co^{4+} ions in these samples where the delithiation is more complete. The concentration of Co^{4+} ions in the sample with $1 - 2y = 0.2$ is so small that it could not be detected by the analysis of the magnetic properties at high temperature, which only revealed that the quasi totality of lithium has been converted in Ni^{4+}. Indeed, the signal associated to Co^{4+} is small in Fig. 12. On another hand it has grown up in the sample with $(1 - 2y) = 0.5$ in Fig. 13, for which we know from the effective magnetic moment that it contains a concentration of 0.07 cobalt ions in the Co^{4+} valence state. We note

however, that this additional line is shifted to a much lower field than expected for a spin with $g = 2$, presumably because of magnetic interactions between Co^{4+} spins and the other magnetic ions.

4. Discussion

$LiNi_yMn_yCo_{1-2y}O_2$ derives from the lamellar $LiMO_2$ oxides with M a 3d element that has been extensively studied in the past, $LiCoO_2$ being still today the most used material in rechargeable Li-ion batteries. The present work brings some enlightenment on the magnetic and structural properties of this family and should then be discussed in this context. First, the analysis of the magnetic properties in ionic intercalation compounds is quantitative, because the orbital momentum is quenched, and the magnetic moment of the ions is reduced to the spin-only value, whether the materials are lamellar like in the present case [36] or olivine compounds [41]. This holds true for ions in the high-spin state of the $3(d^7)$ configuration such as Fe^{2+} [41] or the Ni^{4+} case met in the present work [20,35,36]. This is also true for the Mn^{4+} ion in the $3(d^3)$ configuration [20,26,35,36]. The octahedral environment is obviously favorable for this behavior. For instance, we found that the effective g-factor for the Mn^{4+} ions is $g = 2.0$, which is also the case in other materials where this ion is in the octahedral environment [42,43], but it is not the case when the crystal field symmetry is lower. For instance, a smaller g-value is observed in case of a non-negligible trigonal distortion, like $g = 1.94$ in MnO_2 for instance [44]. Such a quenching of the orbital effects, however, requires that the octahedral crystal field is strong. Indeed, the spin–orbit coupling re-introduces an orbital contribution that is second order in perturbation, i.e. in $[\lambda/(10Dq)]^2$, λ is the spin–orbit coupling and $10Dq$ the splitting energy between the e_g and t_g states. The high-spin configuration implies that the crystal field is not too big; otherwise, the Hund's rule that holds true for free ions is violated, and the low-spin state is stabilized. In the intercalation compounds we are considering here, the lack of any significant orbital contribution suggests that the crystal field is stronger than in most of the solids where these high-spin configurations are met, i.e. that the magnetic ions are close to the spin transition to the low-spin state. This is confirmed by the fact that a spin transition between low- and high-spin states has been observed for Fe^{3+} between the bulk and the surface layer in delithiated Li_xFePO_4 [45]. An additional proof is provided by the cobalt ions. Co^{3+} is in the low spin-state, but Co^{4+} in the delithiated samples is in the high-spin state in the samples we have studied (low Co-concentrations $1 - 2y \leq 0.5$), while in the high concentration limit ($1 - 2y = 1$), it is in the high-spin state in Li_xCoO_2 for $0.94 < x < 1.00$ for samples that are free of impurity [37,46], and in the low-spin state for $0.50 < x < 0.78$ [38]. Ni^{3+} is usually in the low spin state in lamellar compounds. This is known to be the case for instance in $Li_xNi_{0.8}Co_{0.2}O_2$ [4]. It has even been evidenced in $Li_xNi_yMn_yCo_{1-2y}O_2$ in one particular case (no cobalt: $y = 1/2$, partial delithiation: $x = 0.5$) [47]. Note that Ni^{3+} is also in the low-spin sate when it is part of a complex defect $(Li^+ + Ni^{3+})(3a)$ generated when the samples are prepared with an excess of lithium in $Li_xNi_yMn_yCo_{1-2y}O_2$ ($x > 1$) [21,48]. This behavior holds true for ions in the bulk. However, in the surface layer, Ni^{3+} in the high spin state has been observed [24] in the study of the aging upon exposure of samples to humidity in the case $y = 1/3$. The configuration is different, however, for Ni^{4+}. This ion is in the low spin state in $Li_xNi_{0.8}Co_{0.2}O_2$ [4] while it is known to be in the high spin state in $Li_xNi_yMn_yCo_{1-2y}O_2$. Therefore, the introduction of the manganese in the matrix, which was originally made to improve the structural stability of the material, has also as a secondary effect to stabilize the Ni^{4+} ions in the high spin state. One reason might be the fact that the ionic radius of Ni^{4+} is only 0.48 Å in the low-spin state, while it will be the same as the ionic radius of Mn^{4+}, namely 0.53 Å in the high spin state. Therefore, the situation where Ni^{4+} is in the high-spin state is energetically more favorable in our samples where Mn^{4+} ions are in equal quantity, since it avoids a loss in elastic energy in the metal ion sublattice that would have been distorted otherwise. Smaller lattice distortion means a reduced crystal field, which is responsible for the spin transition from low to high spin state is the ground state; but it is also consistent with the fact that there is no local trigonal distortion of the lattice that would have reduced the g-factor associated to Mn^{4+} in the ESR experiments. Nevertheless, the fact that Ni^{4+} has been observed in $Li_xNi_{0.8}Co_{0.2}O_2$ also suggests that the crystal field is still strong enough to make it close to the spin transition.

The ferromagnetism evidenced in these materials is extrinsic in nature, and actually comes from the presence of a small amount of divalent nickel ions in the lithium ($3a$) sites [17,20,23,24]. Note the fact that the determination of [Ni($3a$)] is in quantitative agreement with the result of the Rietveld refinement of the XD spectra is also due to the fact that the orbital contribution of Ni^{2+} and Mn^{4+} are negligible. This ferromagnetic pairing explains why different magnetic behaviors have been reported in the past on such materials. In a pioneer work on this ferromagnetic behavior, Rougier et al. [49] noticed that magnetism is a powerful tool for structure determination of $Li_{1-z}Ni_{1+z}O_2$. While "stoichiometric" $LiNiO_2$ material should not order as a 2-dimensional magnetic lattice geometrically frustrated, these authors gave evidence of ferri- or ferromagnetic phase transition in $Li_{1-z}Ni_{1+z}O_2$ with Tc increasing with z, which reaches 240 K for $z = 0.36$. They related this behavior to the presence of Ni^{2+} in the Li planes of this rhombohedral system, while we argued that the remanent magnetization below Tc in our material is due to the presence of Ni^{2+} ions in the Li sites. The analogy, however, should not be pushed further. In $Li_{1-z}Ni_{1+z}O_2$, Tc is reported to be a transition to a ferrimagnetic order, the net moment responsible for a remanent magnetization below Tc being due to the difference between Ni^{2+} and Ni^{3+} magnetic moments coupled antiferromagnetically through Ni–Ni interactions. In our case, however, we do not have any Ni^{3+} ions present in the material (before delithiation) since the nickel is divalent, and the remanent magnetization is attributable to ferromagnetic Mn^{4+}–O–Ni^{2+}($3a$) interactions.

Another result of the present work is the evidence that the introduction of cobalt in the $LiMO_2$ reduces the presence of Ni^{2+} ions on the lithium sites. Fig. 5 provides us with a simple method to determine the concentration of Ni^{2+}($3a$) ions from the estimation of Tc, by simple (linear) interpolation, and we have found that Ni^{2+}($3a$) ions have been almost eliminated in our samples with a cobalt concentration $(1 - 2y) = 0.5$. This feature also explains that $Li_xNi_{0.8}Co_{0.2}O_2$ has been found to be paramagnetic [4], while $Li_{1-z}Ni_{1+z}O_2$ is ferromagnetic [49]. Since the structure of our material can be viewed as a piling of LiO_6 octahedra planes in alternance with MO_6 planes, the presence of an M ion (Ni^{2+} in the occurrence) on a Li-site, i.e. in the plane of the LiO_6 octahedra, breaks the bidimensional character of the lattice. The reduction of the concentration of Ni^{2+}($3a$) ions by cobalt is thus a confirmation that the substitution of cobalt for nickel tends to increase the 2D structural character in these materials, a result that had previously inferred from a structural study of the $LiNi_{1-y}Co_yO_2$ [50].

The analysis of the magnetic properties has revealed sequential steps in the delithiation process of $LiNi_yMn_yCo_{1-2y}O_2$. The nickel is oxidized first, from Ni^{2+} to $Ni^{3+}$and Ni^{4+}. The cobalt is converted from Co^{3+} to Co^{4+} only after the Nickel has been converted to Ni^{4+}. This result is in agreement with the analysis of the electrochemical properties that we have investigated in the particular case $y = 1/3$, where this sequence was also observed [21]. Indeed, when delithiation is achieved by electrochemical means, it is possible to reach a voltage (>4 V versus Li) where Li can be extracted in the region in the last step where Co^{3+} is converted in Co^{4+}. With the chemical process used in the present work, however, we found impossible

to pursue the delithiation significantly beyond the concentration x where all the nickel ions have been converted in Ni^{4+} (only few % of Co^{4+} could be observed). This situation is often met in these lamellar compounds, as it has been observed in $Li_xCo_{0.8}Mn_{0.2}O_2$ [51].

The analysis of the magnetic properties reported in the present work gives some insight on the electrochemical properties of the same samples, which have been reported in Ref. [52]. In particular, the reduction of the concentration of the Ni($3a$) defects upon the introduction of cobalt in Li(Ni,Mn)O_2 is benefit to the rate capabilities. Also, the delithiation process investigated by charge/discharge curves shows the same dynamics as in the chemical delithiation process: the Ni^{2+} ions are oxidized first, and the oxidation of the cobalt takes places mainly after all of the nickel ions have been converted in Ni^{4+}. Note also that the Mn ions are in the material only to increase the stability of the lattice, but do not play any role in the electrochemical properties. On another hand, the absence of the Mn^{3+} is benefit to the cycling life, since this Jahn-Teller ion generates local deformation and thus internal stress inside the lattice that reduces the cycling life of the battery and its power.

5. Conclusion

The magnetic properties of the $LiNi_yMn_yCo_{1-2y}O_2$ layered material synthesized by wet chemistry via oxalate route have been studied. The analysis of magnetic data allowed us to determine the cationic disorder, i.e. the fraction [Ni($3a$)] of Ni^{2+} ions in the $3a$ lithium sites as a function of the composition y. The spin freezing temperature of the ferromagnetic clusters around Ni^{2+}($3a$) satisfies a linear law $Tc \propto$ [Ni($3a$)] is well satisfied, except for the sample without any cobalt where the concentration of such defects is too large. This law gives a simple way to determine [Ni($3a$)], and gives also a quantitative analysis of the role played by the cobalt to reduce this cation mixing. [Ni($3a$)] decreases monotonically with the cobalt concentration $1-2y$, but becomes negligible only at $1-2y=0.5$, where [Ni($3a$)] is reduced to 0.7%. We find that the delithiation proceeds by different steps. In a first step, Ni^{2+} is converted first in Ni^{3+}, then in Ni^{4+} as x decreases from $x=1$, while Co remains in the Co^{3+} valence state. The analysis of the magnetic properties turns out to be very sensitive, since they allowed us to determine independently the concentration of each metal element in each ionic state.

The electron paramagnetic resonance of $LiNi_yMn_yCo_{1-2y}O_2$ has been measured at different temperatures for different compositions. Ni^{2+} has an integer spin $S=1$, which is not favorable to the observation of the ESR signal. An ESR signal associated to Ni^{2+} impurities can be detected in some materials when the amount of Ni^{2+} is the order of the %. However, when the amount of Ni^{2+} ions is large as it is in the present case, the signal is broaden by local strains, so that no ESR signal associated to this ion can be detected. The paramagnetic resonance detected is attributable to the presence of Mn^{4+} ions that carry a half-integer spin ($S=3/2$) and are then ESR-active.

Acknowledgment

We wish to thank Dr. A. Abdel-Ghany for assistance in the experiments.

References

[1] K. Mizushima, P.C. Jones, P.J. Wiseman, J.B. Goodenough, Mater. Res. Bull. 15 (1980) 783.
[2] R. Rossen, C.D.W. Jones, J.R. Dahn, Solid State Ionics 57 (1992) 311.
[3] M. Wakihara, Mater. Sci. Eng. R 33 (2001) 107.
[4] I. Saadoune, C. Delmas, J. Solid State Chem. 136 (1998) 8.
[5] B.J. Hwang, Y.W. Tsai, C.H. Chen, R. Santhanam, J. Mater. Chem. 13 (2003) 1962.
[6] Z. Lu, R.A. Donaberger, C.L. Thomas, J.R. Dahn, J. Electrochem. Soc. A 149 (2002) 1091.
[7] N. Yabuchi, T. Ohzuku, J. Power Sources 119 (2003) 171.
[8] J.M. Kim, H.T. Chung, Electrochim. Acta 49 (2004) 937.
[9] T.A. Hewston, B.L. Chamberland, J. Phys. Chem. Solids 48 (1987) 97.
[10] Z. Lu, D.D. Mc Neil, J.R. Dahn, Electrochem. Solid State Lett. 4 (2001) A191.
[11] B.J. Hwang, Y.W. Tsai, D. Carlier, G. Ceder, Chem. Mater. 15 (2003) 3676.
[12] K.M. Shaju, G.V. Subba Rao, B.V.R. Chowdari, Electrochim. Acta 48 (2002) 145.
[13] L.S. Cahill, S.C. Yin, A. Samoson, I. Heinmaa, L.F. Nazar, G.R. Goward, Chem. Mater. 17 (2005) 6560.
[14] A. Ait-Salah, K. Zaghib, A. Mauger, F. Gendron, C.M. Julien, Phys. Status Solidi A 203 (2006) R1.
[15] C.M. Julien, A. Ait-Salah, A. Mauger, F. Gendron, Ionics 12 (2006) 11.
[16] M.A. Senaris-Rodriguez, S. Castro-Garcia, A. Castro-Couceiro, C.M. Julien, L.E. Hueso, J. Rivas, Nanotechnology 14 (2003) 277.
[17] X. Zhang, C.M. Julien, A. Mauger, F. Gendron, Solid State Ionics 188 (2011) 148.
[18] X. Zhang, A. Mauger, Q. Lu, H. Groult, L. Perrigaud, F. Gendron, C.M. Julien, Electrochim. Acta 55 (2010) 6440.
[19] A. Abdel-Ghany, K. Zaghib, A. Mauger, F. Gendron, A.E. Eid, H. Abbas, A.M. Hashem, C.V. Ramana, C.M. Julien, Mater. Res. Soc. Symp. Proc. E973 (2007) BB4–BB5.
[20] A. Abdel-Ghany, K. Zaghib, F. Gendron, A. Mauger, C.M. Julien, Electrochim. Acta 52 (2007) 4092.
[21] X. Zhang, W.J. Jiang, A. Mauger, Q. Lu, F. Gendron, C.M. Julien, J. Power Sources 195 (2010) 1292.
[22] D. Hadzi, D. Prevorsek, Spectrochim. Acta 10 (1957) 38.
[23] B. Guarrigues, Tetrahedron 40 (1984) 1151.
[24] X. Zhang, W.J. Jiang, X.P. Zhu, A. Mauger, Q. Lu, C.M. Julien, J. Power Sources 196 (2011) 5102.
[25] A. Abdel-Ghany, A. Mauger, F. Gendron, K. Zaghib, C.M. Julien, ECS Trans. 3–36 (2007) 137.
[26] N. Chernova, M. Ma, J. Xiao, M.S. Whittingham, J. Breger, C.P. Grey, Chem. Mater. 19 (2007) 4682.
[27] A. Abdel-Ghany, K. Zaghib, A. Mauger, M. Massot, F. Gendron, C.V. Ramana, C.M. Julien, ECS Trans. 3–36 (2007) 129.
[28] J.B. Goodenough, Magnetism and the Chemical Bond, Wiley, New York, 1963.
[29] D.D. MacNeil, Z. Lu, J.R. Dahn, J. Electrochem. Soc. A 149 (2002) 1332.
[30] H. Kobayashi, H. Sakaebe, H. Kageyama, K. Tatsumi, Y. Arachi, T. Kamiyama, J. Mater. Chem. 13 (2003) 590.
[31] S. Galam, A. Mauger, Physica A 235 (1997) 573.
[32] M. Escorne, A. Mauger, Phys. Rev. B 35 (1987) 1902.
[33] A. Ben Mahmoud, H. Von Bardeleben, J.L. Cantin, A. Mauger, E. Chikoidze, Y. Dumont, J. Appl. Phys. 101 (2007) 13902.
[34] A. Ben Mahmoud, H. Von Bardeleben, J.L. Cantin, A. Mauger, E. Chikoidze, Y. Dumont, Phys. Rev. B 74 (2006) 115203.
[35] Y. Arachi, H. Kobayashi, S. Emura, Y. Nakata, M. Tanaka, T. Asai, H. Sakaebe, K. Tatsumi, Y. Kagayama, J. Solid State Ionics 176 (2005) 895.
[36] X. Zhang, C. Julien, A. Mauger, F. Gendron, Solid State Ionics 188 (2011) 148.
[37] H.A.M. Abuzeid, A.M.A. Hashem, A.E. Abdel-Ghany, A.E. Eid, A. Mauger, H. Groult, C.M. Julien, J. Power Sources 196 (2011) 6440, and references therein.
[38] J.T. Hertz, Q. Huang, T. McQueen, T. Klimczuk, J.W.G. Bos, L. Viciu, R.J. Cava1, Phys. Rev. B 77 (2008) 075119.
[39] B. Villacampa, R. Alcala, P. Alonso, J.M. Spaeth, J. Phys. Condens. Matter 5 (1993) 747.
[40] R. Stoyanova, E. Zhecheva, R. Alcantara, P. Lavela, J.L. Tirado, Solid State Commun. 102 (1997) 457.
[41] K. Zaghib, A. Mauger, J.B. Goodenough, F. Gendron, C.M. Julien, in: J. Garche (Ed.), Encyclopedia of Electrochemical Power Sources, Five-Volume Set, Elsevier Science, 2009.
[42] M.S. Okubo, F. Elmasry, W. Zhang, M. Fujisawa, T. Sakurai, H. Ohta, M. Azuma, O.A. Sumimova, N. Kumada, J. Phys. Conf. Ser. 200 (2010) 022042.
[43] H.G. Andresen, Phys. Rev. 120 (1960) 1606;
H.G. Andresen, J. Chem. Phys. 35 (1961) 1090.
[44] M. Kakazey, N. Ivanova, Y. Boldurev, S. Ivanov, G. Sokolsky, J.G. Gonzalez-Rodriguez, M. Vlasova, J. Power Sources 114 (2003) 170.
[45] K. Zaghib, A. Mauger, F. Gendron, C.M. Julien, Chem. Mater. 20 (2008) 462.
[46] C. Julien, A. Mauger, H. Groult, X. Zhang, F. Gendron, Chem. Mater. 23 (2011) 208.
[47] Y. Arach, H. Kobayashi, S. Emura, Y. Nakata, M. Tanaka, T. Asai, H. Sakaebe, K. Tatsumi, H. Kageyama, Solid State Ionics 176 (2005) 895.
[48] M. Ma, N.A. Chernova, B.H. Toby, P.Y. Zavalij, M.S. Whittingham, J. Power Sources 165 (2007) 517.
[49] A. Rougier, C. Delmas, G. Chouteau, J. Phys. Chem. Solids 57 (1996) 1101.
[50] A. Rougier, I. Saadoune, P. Gravereau, P. Willmann, C. Delmas, Solid State Ionics 90 (1996) 83.
[51] H.A.M. Abuzeid, A.M.A. Hashem, A.E. Abdel-Ghany, A.E. Eid, A. Mauger, H. Groult, C.M. Julien, J. Power Sources 196 (2011) 6440.
[52] K. Ben Kamel, N. Amdouni, A. Abdel-Ghany, K. Zaghib, A. Mauger, F. Gendron, C.M. Julien, Ionics 14 (2008) 89.